Supporting Information

Multiple-beam interference enabled broadband metamaterial wave plates

Junhao Li,[1] Huijie Guo,[2] Tao Xu,[3] Lin Chen,[1,*] Zhihong Hang,[3] Lei Zhou,[2] and Shuqi Chen[4]

[1]*Wuhan National Laboratory for Optoelectronics, Huazhong University of Science and Technology, Wuhan 430074, China.*
[2] *State Key Laboratory of Surface Physics and Key Laboratory of Micro and Nano Photonic Structures (Ministry of Education), Fudan University, Shanghai 200433, China.*
[3]*College of Physics, Optoelectronics and Energy and Collaborative Innovation Center of Suzhou Nano Science and Technology, Soochow University, Suzhou 215006, China.*
[4]*Laboratory of Weak Light Nonlinear Photonics Ministry of Education School of Physics, Teda Applied Physics Institute, Nankai University, Tianjin 300071, China.*
[*] Corresponding author: chen.lin@mail.hust.edu.cn

Note 1: Derivation process of Eqs. (5) and (6)

The derivation processes of Eqs. (5) and (6) are as follows

$$\begin{aligned}\Delta\phi_1 &= \arg\frac{1}{1-|r_{21}r_{23}|e^{i\phi_c}} \\ &= -\arg(1-|r_{21}r_{23}|\cos\phi_c - i|r_{21}r_{23}|\sin\phi_c) \\ &= \operatorname{arccot}\frac{\frac{1}{|r_{21}r_{23}|}-\cos\phi_{c1}}{\sin\phi_{c1}}\end{aligned} \tag{S1}$$

Then the derivative of $\Delta\phi_1$ with respect to f, is given as

$$\begin{aligned}\tau_{\Delta\phi_1} &= -\frac{1}{1+(\frac{\frac{1}{|r_{21}r_{23}|}-\cos\phi_{c1}}{\sin\phi_{c1}})^2}\frac{d\frac{\frac{1}{|r_{21}r_{23}|}-\cos\phi_{c1}}{\sin\phi_{c1}}}{df} \\ &= -\frac{\sin\phi_{c1}(-\frac{1}{|r_{21}r_{23}|^2}\frac{d|r_{21}r_{23}|}{df}+\sin\phi_c\tau_{\phi_{c1}})-(\frac{1}{|r_{21}r_{23}|}-\cos\phi_{c1})\cos\phi_{c1}\tau_{\phi_{c1}}}{(\sin\phi_{c1})^2+(\frac{1}{|r_{21}r_{23}|}-\cos\phi_{c1})^2} \\ &= \frac{\sin\phi_{c1}\frac{d|r_{21}r_{23}|}{df}+|r_{21}r_{23}|(\cos\phi_{c1}-|r_{21}r_{23}|)\tau_{\phi_{c1}}}{(|r_{21}r_{23}|\sin\phi_{c1})^2+(1-|r_{21}r_{23}|\cos\phi_{c1})^2}\end{aligned} \tag{S2}$$

The functional form of $\Delta\phi_2$ is the same as that of $\Delta\phi_1$. Thus, the derivative function of $\Delta\phi_2$ can be written by replacing the corresponding symbols in Eq. (S2) as

$$\tau_{\Delta\phi_2} = \frac{|r_{34}|\sin\phi_{c2}\frac{d|r_{321}|}{df}+|r_{321}r_{34}|(\cos\phi_{c2}-|r_{321}r_{34}|)\tau_{\phi_{c2}}}{(|r_{321}r_{34}|\sin\phi_{c2})^2+(1-|r_{321}r_{34}|\cos\phi_{c2})^2} \tag{S3}$$

Note 2: Derivation process of $\tau_{\phi_{c2}^x}$ and $\tau_{\phi_{c2}^y}$

$\tau_{\phi_{c2}^x}$ can be written as $\tau_{\phi_{c2}^x} = 2\pi n_3^x h_3^x / c + \tau_{\phi_{r321}^x}$, since $\phi_{c2}^x = 2k_3^x h_3^x + \phi_{r_{321}}^x$. According to Eq. (2) of the main text, $r_{321}^x = r_{32}^x + t_{32}^x r_{21}^x t_{23}^x e^{2ik_2^x h_2} / (1 - r_{21}^x r_{23}^x e^{2ik_2^x h_2})$. By incorporating $r_{32}^x = -r_{23}^x$ and $t_{32}^x t_{23}^x = 1 - (r_{23}^x)^2$ into $r_{321}^x = r_{32}^x + t_{32}^x r_{21}^x t_{23}^x e^{2ik_2^x h_2} / (1 - r_{21}^x r_{23}^x e^{2ik_2^x h_2})$, r_{321}^x can be reduced to $r_{321}^x = (-r_{23}^x + r_{21}^x e^{2ik_2^x h_2}) / 1 - r_{21}^x r_{23}^x e^{2ik_2^x h_2}$ and its argument can thus be represented by

$$\begin{aligned}\phi_{r_{321}}^x &= \arg \frac{-r_{23}^x + r_{21}^x e^{2ik_2^x h_2}}{1 - r_{21}^x r_{23}^x e^{2ik_2^x h_2}} \\ &= \arg \frac{-r_{23}^x + r_{21}^x \cos\phi_{c1}^x + i r_{21}^x \sin\phi_{c1}^x}{1 - r_{21}^x r_{23}^x \cos\phi_{c1}^x - i r_{21}^x r_{23}^x \sin\phi_{c1}^x} \\ &= \arctan \frac{r_{21}^x \sin\phi_{c1}^x}{-r_{23}^x + r_{21}^x \cos\phi_{c1}^x} - \arctan \frac{r_{21}^x r_{23}^x \sin\phi_{c1}^x}{1 - r_{21}^x r_{23}^x \cos\phi_{c1}^x}\end{aligned} \tag{S4}$$

$$\begin{aligned}\tau_{\phi_{r321}^x} &= \frac{\dfrac{d \dfrac{r_{21}^x \sin\phi_{c1}^x}{-r_{23}^x + r_{21}^x \cos\phi_{c1}^x}}{df}}{1 + \left(\dfrac{r_{21}^x \sin\phi_{c1}^x}{-r_{23}^x + r_{21}^x \cos\phi_{c1}^x} \right)^2} - \frac{\dfrac{d \dfrac{r_{21}^x r_{23}^x \sin\phi_{c1}^x}{1 - r_{21}^x r_{23}^x \cos\phi_{c1}^x}}{df}}{1 + \left(\dfrac{r_{21}^x r_{23}^x \sin\phi_{c1}^x}{1 - r_{21}^x r_{23}^x \cos\phi_{c1}^x} \right)^2} \\ &= \left[\frac{-r_{21}^x r_{23}^x \cos\phi_{c1}^x + (r_{21}^x)^2}{(-r_{23}^x + r_{21}^x \cos\phi_{c1}^x)^2 + (r_{21}^x \sin\phi_{c1}^x)^2} - \frac{r_{21}^x r_{23}^x \cos\phi_{c1}^x - (r_{21}^x r_{23}^x)^2}{(1 - r_{21}^x r_{23}^x \cos\phi_{c1}^x)^2 + (r_{21}^x r_{23}^x \sin\phi_{c1}^x)^2} \right] \tau_{\phi_{c1}^x}\end{aligned} \tag{S5}$$

Since cavity one interferes constructively along the x-polarization direction, we can get $\cos\phi_{c1}^x = 1$ and $\sin\phi_{c1}^x = 0$. By substituting $\cos\phi_{c1}^x$ and $\sin\phi_{c1}^x$ into Eq. (S5), we can get $\tau_{\phi_{r321}^x} = r_{21}^x [1 - 2r_{21}^x r_{23}^x + (r_{23}^x)^2] / [(r_{21}^x - r_{23}^x)(1 - r_{21}^x r_{23}^x)] \tau_{\phi_{c1}^x}$. Then, $\tau_{\phi_{c2}^x}$ can be written as

$$\tau_{\phi_{c2}^x} = \frac{2\pi n_3^x h_3}{c} + \frac{r_{21}^x [1 - 2r_{21}^x r_{23}^x + (r_{23}^x)^2]}{(r_{21}^x - r_{23}^x)(1 - r_{21}^x r_{23}^x)} \tau_{\phi_{c1}^x} \tag{S6}$$

$\tau_{\phi_{c2}^y}$ can be written by replacing the corresponding symbols of Eq. (S5):

$$\tau_{\phi_{r321}^y} = \left[\frac{-r_{21}^y r_{23}^y \cos\phi_{c1}^y + (r_{21}^x)^2}{(-r_{23}^y + r_{21}^y \cos\phi_{c1}^y)^2 + (r_{21}^y \sin\phi_{c1}^y)^2} - \frac{r_{21}^y r_{23}^y \cos\phi_{c1}^y - (r_{21}^y r_{23}^y)^2}{(1 - r_{21}^y r_{23}^y \cos\phi_{c1}^y)^2 + (r_{21}^y r_{23}^y \sin\phi_{c1}^y)^2} \right] \tau_{\phi_{c2}^y} \tag{S7}$$

Since cavity one interferes destructively along the y-polarization direction, we can get $\cos\phi_{c1}^y = -1$ and $\sin\phi_{c1}^y = 0$. By substituting $\cos\phi_{c1}^y$ and $\sin\phi_{c1}^y$ into Eq. (S7), we can get that $\tau_{\phi_{r321}^y} = r_{21}^y [1 - 2r_{21}^y r_{23}^y + (r_{23}^y)^2] / [(r_{21}^y - r_{23}^y)(1 - r_{21}^y r_{23}^y)] \tau_{\phi_{c1}^y}$. Then, $\tau_{\phi_{c2}^y}$ can be written as

$$\tau_{\phi_{c2}^y} = \frac{2\pi n_3^y h_3}{c} + \frac{r_{21}^y [1 + 2r_{21}^y r_{23}^y + (r_{23}^y)^2]}{(r_{21}^y + r_{23}^y)(1 + r_{21}^y r_{23}^y)} \tau_{\phi_{c1}^y} \tag{S8}$$

Note 3: Theoretical calculation of the dispersion relation of the SSP mode supported by a one-dimensional anisotropic MTM composed of metal/dielectric multilayer

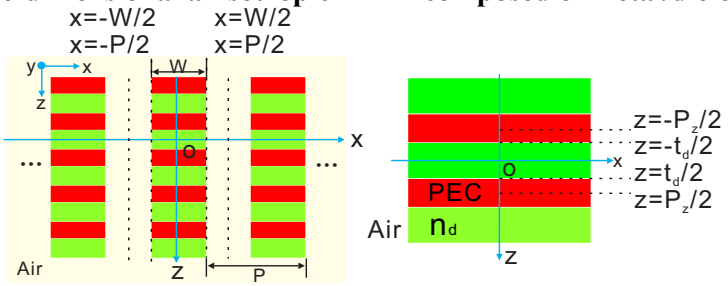

FIG. S1. Schematic of the one-dimensional anisotropic MTM. The anisotropic MTM is composed of alternating metal/dielectric multilayer with finite width, W, surrounded with air. The thicknesses of metal and dielectric layers are represented by t_m, and t_d, respectively, and the lattice constant along z direction is denoted as P_z $(=t_m+t_d)$. The lattice constant along x direction is represented by P. In the microwave and terahertz domain, the metal can be treated as perfect electric conductor.

We firstly write out the EM fields in all the regions except in the metal region:

$$E_z=\begin{cases}[\rho_+e^{ik_zz}e^{ik_xx}+\rho_-e^{ik_zz}e^{-ik_xx}]/\sqrt{P_z} & (-P/2<x<-W/2)\\ [\rho_+'e^{ik_zz}e^{ik_xx}+\rho_-'e^{ik_zz}e^{-ik_xx}]/\sqrt{P_z} & (W/2<x<P/2)\end{cases} \tag{S9}$$

$$H_y=\begin{cases}k_0[-\rho_+e^{ik_zz}e^{ik_xx}+\rho_-e^{ik_zz}e^{-ik_xx}]/(k_x\sqrt{P_z}) & (-P/2<x<-W/2)\\ k_0[-\rho_+'e^{ik_zz}e^{ik_xx}+\rho_-'e^{ik_zz}e^{-ik_xx}]/(k_x\sqrt{P_z}) & (W/2<x<P/2)\end{cases} \tag{S10}$$

$$E_z=\begin{cases}[C_+e^{in_dk_0x}+C_-e^{-in_dk_0x}]/\sqrt{t_d} & (-t_d/2<z<t_d/2,|x|<W/2)\\ 0 & (t_d/2<|z|<P_z/2,|x|<W/2)\end{cases} \tag{S11}$$

$$H_y=[-n_dC_+e^{in_dk_0x}+n_dC_-e^{-in_dk_0x}]/\sqrt{t_d} \quad (-t_d/2<z<t_d/2,|x|<W/2) \tag{S12}$$

where $\rho_\pm$, $\rho_\pm'$ and $C_\pm$ are unsolved coefficients related to mode amplitudes in different regions.

One can connect Eqs. (S9)-(S12) with the Maxwell's boundary conditions and the periodic boundary conditions, yielding the following relations

$$\begin{cases}\rho_+\phi_-+\rho_-\phi_+=(C_+\phi_-'+C_-\phi_+')S_0 & (E_z,x=-W/2)\\ \rho_+'\phi_++\rho_-'\phi_-=(C_+\phi_+'+C_-\phi_-')S_0 & (E_z,x=W/2)\\ \rho_+\phi_-S_0k_0/k_x-\rho_-\phi_+S_0k_0/k_x=(C_+\phi_-'-C_-\phi_+')n_d & (H_y,x=-W/2)\\ \rho_+'\phi_+S_0k_0/k_x-\rho_-'\phi_-S_0k_0/k_x=(C_+\phi_+'-C_-\phi_-')n_d & (H_y,x=W/2)\\ \rho_+\phi_-^P+\rho_-\phi_+^P=\rho_+'\phi_+^P+\rho_-'\phi_-^P & (E_z,|x|=P/2)\\ \rho_+\phi_-^P-\rho_-\phi_+^P=\rho_+'\phi_+^P-\rho_-'\phi_-^P & (H_y,|x|=P/2)\end{cases} \tag{S13}$$

where $\phi_\pm=e^{\pm ik_xW/2}$, $\phi_\pm'=e^{\pm in_dk_0W/2}$, $\phi_\pm^P=e^{\pm ik_xP/2}$ and $S_0=\sqrt{t_d/P_z}\,\sin(k_zt_d/2)/(k_zt_d/2)$.

By eliminating $\rho_\pm$, $\rho_\pm'$ and $C_\pm$ in Eq. (S13), we obtain

$$\pm A_-[\tan(\frac{n_dk_0W}{2})-\tan(\frac{k_xg}{2})]=A_+[\tan(\frac{n_dk_0W}{2})+\tan(\frac{k_xg}{2})] \tag{S14}$$

where $g=P-W$ and $A_\pm=k_0S_0^2/k_x\pm n_d$:

(1) If $A_{-}[\tan(n_d k_0 W/2)-\tan(k_x g/2)]=A_{+}[\tan(n_d k_0 W/2)+\tan(k_x g/2)]$, then $-n_d\tan(n_d k_0 W/2)=(k_0/k_x)S_0^2\tan(k_x g/2)$. By using $k_x=i\sqrt{k_z^2-k_0^2}$, the dispersion relation can be expressed as

$$\sqrt{k_z^2-k_0^2}=-k_0 S_0^2\frac{1-e^{-\sqrt{k_z^2-k_0^2}g}}{1+e^{-\sqrt{k_z^2-k_0^2}g}}\cot(\frac{n_d k_0 W}{2})/n_d \qquad \text{(S15)}$$

for asymmetrical SSP mode. As $g\to+\infty$, $(1-e^{-\sqrt{k_z^2-k_0^2}g})\big/(1+e^{-\sqrt{k_z^2-k_0^2}g})\to 1$, Eq. (S15) will be reduced to the dispersion relation for the asymmetrical SSP mode.

(2) If $-A_{-}[\tan(n_d k_0 W/2)-\tan(k_x g/2)]=A_{+}[\tan(n_d k_0 W/2)+\tan(k_x g/2)]$, then $-n_d\tan(k_x g/2)=(k_0/k_x)S_0^2\tan(n_d k_0 W/2)$. By using $k_x=i\sqrt{k_z^2-k_0^2}$, we can get

$$\sqrt{k_z^2-k_0^2}=k_0 S_0^2\frac{1+e^{-\sqrt{k_z^2-k_0^2}g}}{1-e^{-\sqrt{k_z^2-k_0^2}g}}\tan(\frac{n_d k_0 W}{2})/n_d \qquad \text{(S16)}$$

for symmetrical SSP mode. As $g\to+\infty$, $(1-e^{-\sqrt{k_z^2-k_0^2}g})\big/(1+e^{-\sqrt{k_z^2-k_0^2}g})\to 1$, Eq. (S16) will be reduced to the dispersion relation for the symmetrical SSP mode.

The calculated dispersion curves [Fig. S2(a)] and electric field diagrams [Fig. S2(b)] notably reflect the coupling effect of the SSP modes between the adjacent units. A higher effective refractive index of the SSP mode could be achieved by tuning the geometrical parameters of the anisotropic MTM or using a smaller gap separation to enhance the coupling between the adjacent SSP modes. It should be noted here, despite the great capability of the asymmetrical SSP mode in tuning the dispersion relation, it is not suitable for the design of functional devices due to zero coupling with the incident waves.

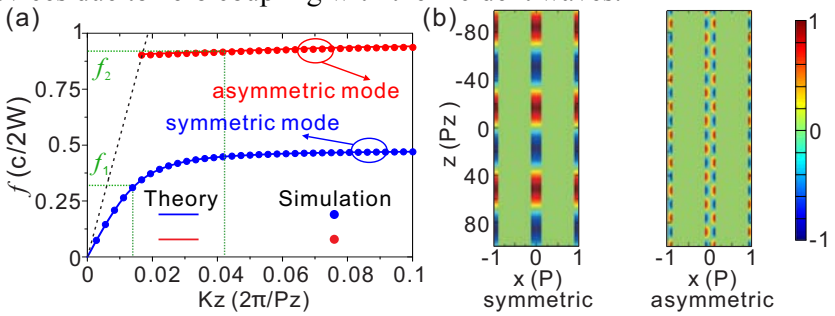

FIG. S2. Dispersion curves and field distributions of symmetric and asymmetric SSP modes of one dimensional anisotropic MTM. (a) Dispersion curves calculated for $t_m=0.04$ mm, $t_d=0.2$ mm, $w=6$ mm, $P=8$ mm, and $n_d=2.07$. (b) Distributions of the real part of E_x of symmetric and asymmetric SSP modes for the 1D anisotropic MTM at $f_1=0.32(c/2W)$ and $f_2=0.92(c/2W)$, respectively.

Note 4: The broadband QWP in the terahertz regime

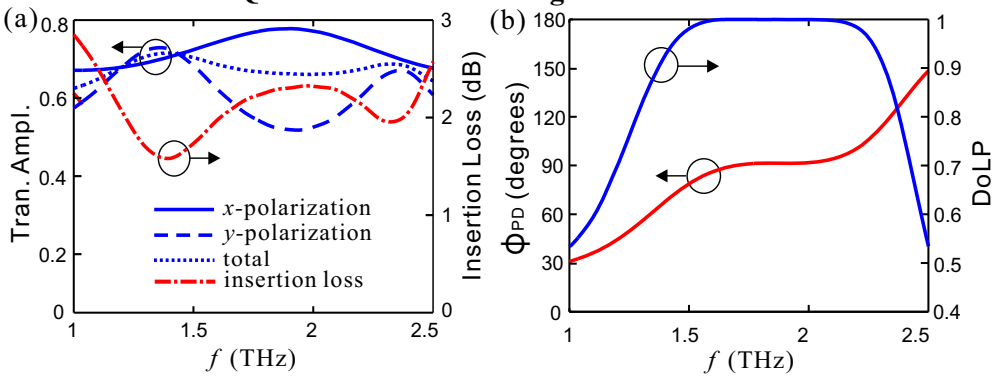

FIG. S3. (a) Transmission amplitudes for the x- and y- polarizations, total transmission amplitude, and insertion loss versus f. (b) ϕ_{PD} (red) and DoLP (blue) as a function of f.

For the broadband QWP in the terahertz regime, the anisotropic MTM is composed of Al/GaAs multilayer ($n_{\mathrm{GaAs}} = 3.6$). Each Al and GaAs layer is with a thickness of $t_d = 0.5$ μm and $t_m = 0.5$ μm, respectively. There are 40 pairs of Al/GaAs layers, resulting in a total thickness of 40 μm for the anisotropic MTM ($h_2 = 40$ μm). The cross-sectional dimension of the anisotropic MTM is set as $Wx = 9$ μm and $Wy = 10.8$ μm, and the lattice constants along the x- and y- axes are $Px = Py = 12$ μm. The anisotropic MTM is deposited on a semi-infinite PDFE substrate with the refractive index of $n_3 = 1.38$.

We designed the structural parameters to make constructive interference for x polarization and destructive interference for y-polarization encounter at around 1.9 THz. It can be inferred from the transmission amplitudes in Fig. S3(a) that $\left|t_{123}^{x}\right|$ and $\left|t_{123}^{y}\right|$ reaches the maximum and minimum values at around 1.9 THz, respectively. The designed QWP can keep the cross-polarization phase difference, ϕ_{PD}, within the range of 90±10° over a wide wavelength band of 1.51–2.19 THz (dispersionless band), 35.8% with respect to 1.9 THz [Fig. S3(b)]. The total transmission amplitude ($\sqrt{(\left|t_{123}^{x}\right|^2 + \left|t_{123}^{y}\right|^2)/2}$) reaches up to approximately 65% [Fig. S3(a)], associated with the insertion loss of less than 2.4 dB [Fig. S3(a)], and the DoLP is above 98% [Fig. S3(b)] in the dispersionless band.